

Diffractive Dissociation from Non-Linear Evolution in DIS on Nuclei

E. Levin^{*} ^{a),b)} and M. Lublinsky[†] ^{a)}

^{a)} *HEP Department*

School of Physics and Astronomy

Raymond and Beverly Sackler Faculty of Exact Science

Tel Aviv University, Tel Aviv, 69978, ISRAEL

^{b)} *DESY Theory Group*

22603, Hamburg, GERMANY

May 21, 2019

Abstract

The process of single diffractive dissociation off nuclei is considered on a basis of solutions to the nonlinear evolution equation. The relevant saturation scales $Q_{sA}^D(x, x_0)$ are determined and their dependences on Bjorken x , atomic number A , and minimal rapidity gap $Y_0 \equiv \ln 1/x_0$ are investigated. The solutions are shown to possess the geometrical scaling in a broad kinematic region for x well below x_0 . A detailed theoretical discussion of saturation scale and scaling is presented.

The ratio $\sigma^{diff}/\sigma^{tot}$ is computed for several nuclei. We predict that at $x \simeq 10^{-4}$ this ratio is of the order 25% which is much larger to the one of proton. This result indicates a possibility to observe a very strong nuclear shadowing.

^{*}e-mail: leving@post.tau.ac.il

[†]e-mail: mal@post.tau.ac.il mal@tx.technion.ac.il

1 Introduction

During the last years there has been a significant growth in interest to a new phase of QCD associated with high parton density [1, 2]. This interest is mostly related to availability of new low x $e - p$ DIS data. Another source of information on QCD dynamics at high parton density is due to nuclei which can provide high density effects at comparatively lower energies. The researches on nuclear shadowing has been recently accelerated due to the start of RHIC collider.

In the present paper we concentrate on single diffraction dissociation off nuclei which plays an important role in revealing QCD dynamics at high parton density. Diffractive inclusive production in DIS is believed to be quite sensitive to the shadowing effects [3] and, in fact, is a measure of these effects due to the AGK cutting rules [4]. We are going to investigate the cross section of diffractive dissociation at fixed impact parameter and as a final result compute the ratio of the total inclusive diffraction to the total inclusive production in DIS off nuclei.

The total deep inelastic cross section is related to the dipole cross section

$$\sigma(x, Q^2) = \int d^2 r_{\perp} \int dz |\Psi^{\gamma^*}(Q^2; r_{\perp}, z)|^2 \sigma_{\text{dipole}}(r_{\perp}, x), \quad (1.1)$$

where the QED wave functions Ψ^{γ^*} of the virtual photon are well known [5, 6, 7]. In its turn, the dipole cross section is given by the integral over the impact parameter b :

$$\sigma_{\text{dipole}}(r_{\perp}, x) = 2 \int d^2 b N(r_{\perp}, x; b), \quad (1.2)$$

where N stands for imaginary part of the dipole-target interaction amplitude for dipole of the size r_{\perp} scattered elastically at the impact parameter b . This function is a subject to a nonlinear quantum evolution equation first derived by Balitsky and Kovchegov (BK) [8, 9]. The BK equation was studied both asymptotically [2] and numerically [10, 11] though for the purposes of the present paper we will use a numerical solution of this equation obtained in Ref. [12].

The total cross section of single diffractive dissociation is defined similarly:

$$\sigma(x, Q^2) = \int d^2 r_{\perp} \int dz |\Psi^{\gamma^*}(Q^2; r_{\perp}, z)|^2 \sigma_{\text{dipole}}^{\text{diff}}(r_{\perp}, x), \quad (1.3)$$

and

$$\sigma_{\text{dipole}}^{\text{diff}}(r_{\perp}, x, x_0) = 2 \int d^2 b N^D(r_{\perp}, x, x_0; b). \quad (1.4)$$

The function N^D is a partial cross section for the dipole-target diffractive scattering with the minimal rapidity gap $Y_0 = \ln 1/x_0$. A nonlinear quantum evolution equation for N^D was derived in Ref. [13] and then rederived in Ref. [14]:

$$\begin{aligned}
N^D(\mathbf{x}_{01}, Y, Y_0; b) &= N^2(\mathbf{x}_{01}, Y_0; b) e^{-\frac{4C_F\alpha_S}{\pi} \ln(\frac{\mathbf{x}_{01}}{\rho})(Y-Y_0)} + \frac{C_F\alpha_S}{\pi^2} \int_{Y_0}^Y dy e^{-\frac{4C_F\alpha_S}{\pi} \ln(\frac{\mathbf{x}_{01}}{\rho})(Y-y)} \\
&\times \int_{\rho} d^2\mathbf{x}_2 \frac{\mathbf{x}_{01}^2}{\mathbf{x}_{02}^2 \mathbf{x}_{12}^2} \left[2 N^D(\mathbf{x}_{02}, y, Y_0; \mathbf{b} - \frac{1}{2}\mathbf{x}_{12}) + N^D(\mathbf{x}_{02}, y, Y_0; \mathbf{b} - \frac{1}{2}\mathbf{x}_{12}) N^D(\mathbf{x}_{12}, y, Y_0; \mathbf{b} - \frac{1}{2}\mathbf{x}_{02}) \right. \\
&\left. - 4 N^D(\mathbf{x}_{02}, y, Y_0; \mathbf{b} - \frac{1}{2}\mathbf{x}_{12}) N(\mathbf{x}_{12}, y; \mathbf{b} - \frac{1}{2}\mathbf{x}_{02}) + 2 N(\mathbf{x}_{02}, y; \mathbf{b} - \frac{1}{2}\mathbf{x}_{12}) N(\mathbf{x}_{12}, y; \mathbf{b} - \frac{1}{2}\mathbf{x}_{02}) \right].
\end{aligned} \tag{1.5}$$

The lhs. of Eq. (1.5) is a partial cross section of the diffractive dissociation for dipole of the size $r_{\perp} \equiv \mathbf{x}_{01} \equiv |\mathbf{x}_0 - \mathbf{x}_1|$ and rapidity $Y \equiv \ln 1/x$. The rhs. of Eq. (1.5) describes quantum evolution in which the original dipole first splits to two dipoles and then the latter scatter off the target.

When rapidity fills the whole rapidity gap $Y = Y_0$ diffraction is given by a pure elastic interaction

$$N^D(r_{\perp}, x_0, x_0; b) = N^2(r_{\perp}, x_0; b). \tag{1.6}$$

Eq. (1.6) serves as initial condition to the evolution (1.5).

For the first time a numerical solution of Eq. (1.5) was found and investigated in Ref. [16] for a proton target. In the following paper [17] the ratio $\sigma^{diff}/\sigma^{tot}$ was computed and in a certain kinematic domain shown to be energy independent in agreement with the HERA data [15]. In the present paper we report on the numerical solution of Eq. (1.5) for nucleus targets and repeat the program of Refs. [16, 17].

The paper is organized as follows. In the next Section (2) we present solutions of Eq. (1.5) for various nuclei. Section 3 is devoted to the determination of the saturation scale and its properties. Geometrical scaling is studied in Section 4. The ratio $\sigma^{diff}/\sigma^{tot}$ is computed in Section 5. Section 6 present a theoretical discussion of the saturation scale. The last Section (7) is concluding.

2 Solution of the non-linear equation

In this section we report on the numerical solution of the equation (1.5) for various nuclear targets. We consider six real nuclei: Ne_{20} , Ca_{40} , Zn_{70} , Mo_{100} , Nd_{150} , and Au_{197} . All the details about nuclear profile functions are borrowed from Ref. [18] and are summarized in our paper [12]. As in the series of our previous papers the method of iterations proposed in Ref. [11] is applied. The constant value for the strong coupling constant $\alpha_S = 0.25$ is always used. The solutions are computed for $10^{-4} \leq x_0 \leq 10^{-2}$ and within the kinematic region $10^{-7} \leq x \leq x_0$ and distances up to a few fermi.

The function N_A^D is formally a function of four variables: the energy gap x_0 , the energy variable x , the transverse distance r_{\perp} , and the impact parameter b . In order to simplify the problem we will proceed similarly to the treatment of the b -dependence of the function N_A [12] and N^D for

proton [16]. Namely, we use the anzats which preserves the very same b -dependence as introduced in the initial conditions:

$$N_A^D(r_\perp, x, x_0; b) = (1 - e^{-\kappa_A^D(x, x_0, r_\perp) S_A(b)/S_A(0)})^2, \quad (2.7)$$

with

$$\kappa_A^D(x, x_0, r_\perp) = -\ln(1 - \sqrt{\tilde{N}_A^D(r_\perp, x, x_0)}). \quad (2.8)$$

$\tilde{N}_A^D(r_\perp, x, x_0)$ represents a solution of the equation (1.5) but with no dependence on the forth variable. The initial conditions for the function $\tilde{N}_A^D(r_\perp, x, x_0)$ are set at $b = 0$.

Fig. 1 shows the solutions \tilde{N}_A^D as a function of the transverse distance for various values of x at fixed $x_0 = 10^{-2}$. The obtained curves reproduce the very same pattern as for the case of a proton target [16]. The results for different nuclei can be used in order to study the A dependence of the diffraction dissociation. In agreement with all expectations, the unitarity bound $N_A^D = 1$ is reached first by the most heavy nucleus. The dependence of the solutions on the gap variable x_0

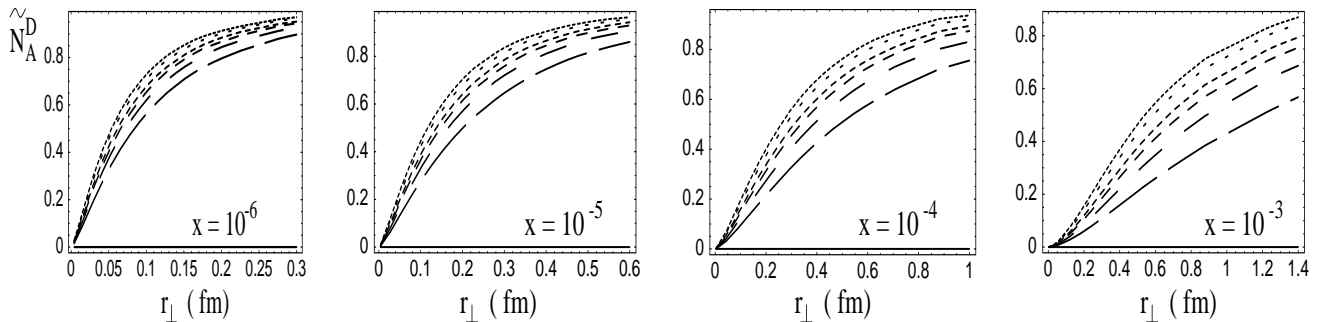


Figure 1: The function $\tilde{N}_A^D(x_0 = 10^{-2})$ is plotted versus transverse distance. The curves correspond to different nuclei (from up to down): Au, Nd, Mo, Zn, Ca, Ne.

is very weak and quite similar to the proton case of Ref. [16].

3 Saturation Scale

Determination of the diffractive saturation scale $Q_s^D(A, x, x_0)$ from the solution \tilde{N}_A^D is a subject of this section. Following the same spirit of our previous works [11, 12, 20, 16] we introduce several definitions of the saturation scale while the variety of the obtained results will indicate the uncertainty in the definitions.

For the step like function it is natural to define the saturation scale as position where $\tilde{N}_A^D = 1/2$:

- **Definition (a):**

$$\tilde{N}_A^D(R_s^D, x, x_0) = 1/2, \quad Q_s^D \equiv 2/R_s^D. \quad (3.9)$$

The equality between the saturation radius R_s^D and the saturation momentum Q_s^D is motivated by the double logarithmic approximation. Though this approximation is formally not justified, we still believe it to make reliable estimates provided Q_s^D is large enough. The definition (3.9) is analogous to the one proposed in Ref. [11] $N(2/Q_s, x) = 1/2$. If we recall that $N_A^D = N_A^2$ at $x = x_0$ and postulate $Q_s^D(A, x_0, x_0) = Q_s(A, x_0)$ then we should require

• **Definition (b):**

$$\tilde{N}_A^D(2/Q_s^D, x, x_0) = 1/4. \quad (3.10)$$

An alternative definition of the saturation scale could be one motivated by the Glauber-Mueller formula [6] for $N_A(r_\perp, x)$

$$N_A(r_\perp, x, x_0; b) = (1 - e^{-\kappa_A(r_\perp, x, x_0) S_A(b)}) , \quad (3.11)$$

with

$$\kappa_A = \frac{3\pi^2 \alpha_S}{4} r_\perp^2 A x G(x, \frac{4}{r_\perp^2}) , \quad (3.12)$$

with xG standing for gluon density of a nucleon.

• **Definition (c):**

$$\kappa_A^D(2/Q_s^D, x, x_0) = 1/2. \quad (3.13)$$

The saturation scales obtained through the above definitions are depicted in Fig. 2 for $x_0 = 10^{-2}$ and in Fig. 3 for $x_0 = 10^{-3}$. The saturation scale is clearly almost x_0 independent. The

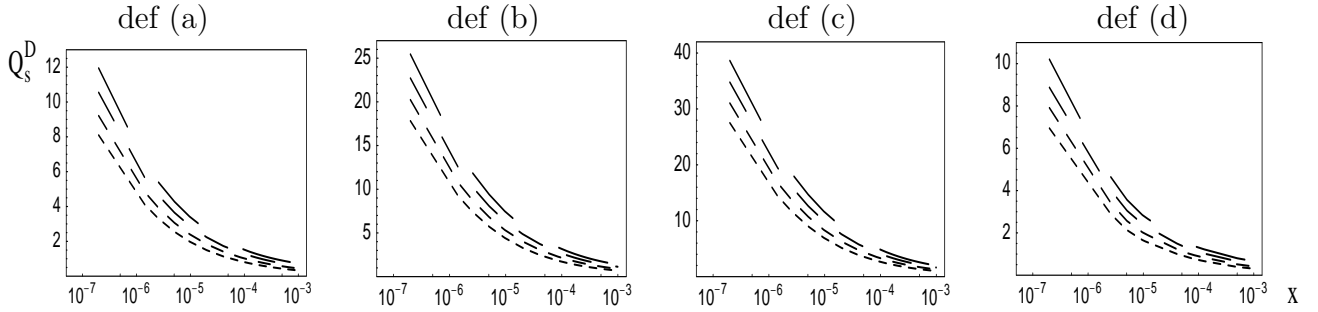


Figure 2: The saturation scale $Q_s^D(x_0 = 10^{-2})$ is plotted versus x . The curves correspond to (from up to down) Au, Mo, Ca, and Ne.

definition (d) is related to the scaling properties of the function N_A^D and will be discussed in the next section.

It is important to learn about the x and A dependencies of the saturation scale. To this goal, we assume the following parameterization:

$$Q_s^D(A, x, x_0) = Q_{s0}^D(x_0) A^p x^{-\lambda}. \quad (3.14)$$

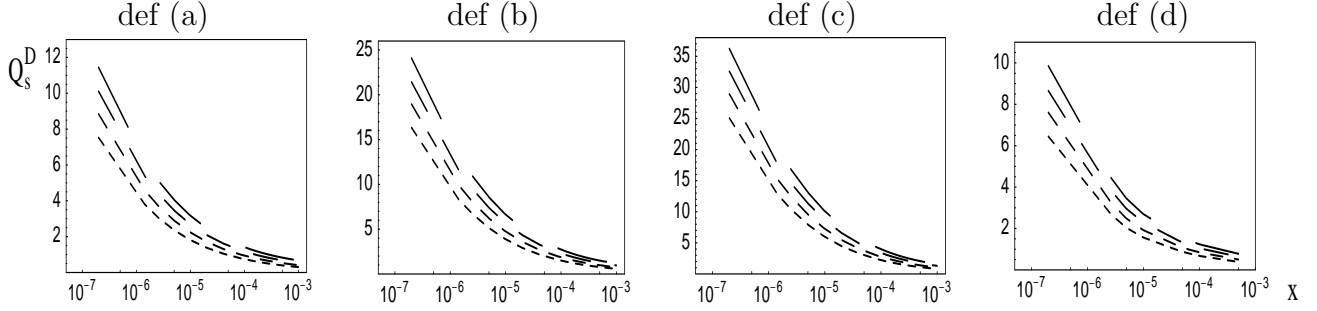


Figure 3: The saturation scale $Q_s^D(x_0 = 10^{-3})$ is plotted versus x . The curves correspond to (from up to down) Au, Mo, Ca, and Ne.

Nuclei \ x	10^{-7}	10^{-6}	10^{-5}	10^{-4}	10^{-3}
Light	0.15	0.20	0.24	0.29	0.35
Heavy	0.15	0.19	0.22	0.25	0.29
All	0.15	0.19	0.23	0.27	0.32

Table 1: The power $p(x)$ for various values of x .

In fact, the parameterization (3.14) is a good approximation for the values of the saturation scales obtained with

$$\lambda = 0.37 \pm 0.04,$$

and p given in Table 1. All the values in the table are central values given with errors less than 10%.

The x_0 -dependence of the saturation scale is very weak. If we try to use the power law parameterization $Q_{s0}^D \sim x_0^\beta$ then $\beta = 0.055 \pm 0.035$. The large error reflects a significant x -dependence of β as well as its sensitivity to the saturation scale definition.

It is important to stress that the obtained power λ coincides with the corresponding power of the saturation scales Q_s [20] and Q_s^D [16].

4 Geometrical Scaling

In Ref. [20] the function \tilde{N} was shown to display phenomena of geometrical scaling while Ref. [16] presents a detailed analysis of the scaling for the proton partial cross section \tilde{N}^D . As can be expected, the function \tilde{N}_A^D displays the very same property and in this section we give a brief illustration of the phenomena. In the saturation region the scaling implies the amplitude to be a function of only one variable $\tau = r_\perp^2 \cdot Q_s^D(A, x, x_0)$:

$$\tilde{N}_A^D(r_\perp, x, x_0) = \tilde{N}_A^D(\tau) \quad (4.15)$$

Define the following derivative functions assuming the scaling behavior (4.15):

$$N_y^D(r_\perp, A, x, x_0) \equiv -\frac{\partial \tilde{N}_A^D}{\partial Y} = \frac{d\tilde{N}_A^D}{d\tau} \tau \frac{\partial \ln(Q_s^D)^2}{\partial \ln x}, \quad (4.16)$$

$$N_r^D(r_\perp, A, x, x_0) \equiv r_\perp^2 \frac{\partial \tilde{N}_A^D}{\partial r_\perp^2} = \frac{d\tilde{N}_A^D}{d\tau} \tau, \quad (4.17)$$

$$\Re(r_\perp, A, x, x_0) \equiv -\frac{\partial \tilde{N}_A^D}{\partial Y_0} = \frac{d\tilde{N}_A^D}{d\tau} \tau \frac{\partial \ln(Q_s^D)^2}{\partial \ln x_0}. \quad (4.18)$$

If the scaling behavior (4.15) takes place indeed, then both the ratios N_y^D/N_r^D and \Re/N_r^D are r_\perp independent functions.

Let us first consider scaling with respect to x . Fig. 4 presents the derivatives N_y^D and N_r^D as functions of transverse distance r_\perp at fixed $x_0 = 10^{-2}$. Both functions N_y^D and N_r^D have extremum

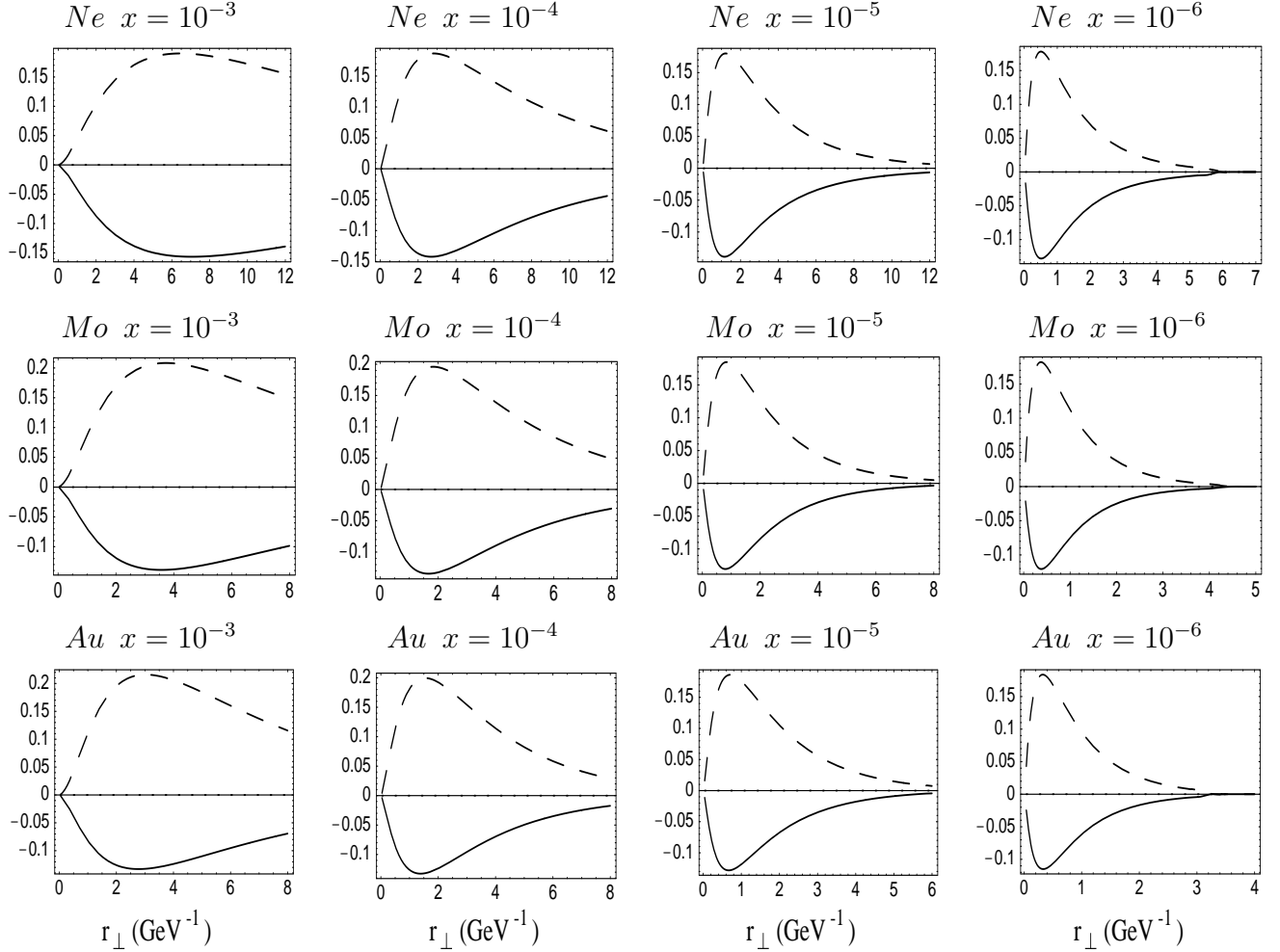


Figure 4: The derivative functions N_r^D (dashed line) and N_y^D (solid line) as functions of transverse distance at fixed $x_0 = 10^{-2}$.

placed at the same distance depending on x and atomic number A . This is a consequence of the scaling behavior (4.15) and equations (4.16) and (4.17). The extremum occurs at certain τ_{max} , such that $\tilde{N}_A^{D'}(\tau_{max}) = -\tau_{max} \tilde{N}_A^{D''}(\tau_{max})$. In Fig. 4 τ_{max} is approached by varying r_\perp at fixed x . Alternatively it can be reached by varying x at fixed r_\perp .

The position of the maximum τ_{max} can be used as yet another definition of the saturation scale:

• **Definition (d):**

$$\tau(r_{\perp} = 2/Q_s^D) = \tau_{max}. \quad (4.19)$$

The saturation scale due to the above definition is presented on Figs. 2 and 3.

In order to be brief we skip graphs representing the ratios N_y^D/N_r^D and \mathfrak{R}/N_r^D . As expected, the r_{\perp} independence of the ratios is approximately reproduced. Thus the scaling with respect to x variable is established. Within relative error of order 20% the resulting ratios do not depend neither on x no the atomic number A . This observation is consistent with the power law anzats for the saturation scale (3.14) and the conclusions of the previous section. The results on the scaling practically do not alter when x_0 is varied.

5 $\sigma^{diff}/\sigma^{tot}$

In this section we consider a ratio of the total inclusive diffractive dissociation to total inclusive production. The mass maximally produced in diffractive process can be expresses through the minimal rapidity gap $Y_0 = \ln 1/x_0$:

$$M^2 = Q^2 (x_0/x - 1).$$

At $x = x_0$ diffraction is given by pure elastic scattering. We set $x_0 = 10^{-2}$ as a minimal gap allowed in our calculations.

Fig. (5) display the ratio as a function of x for fixed values of the photon virtuality Q^2 . This ratio indicates a value of shadowing corrections. The ratio grows as x decreases tending to the unitarity bound $1/2$. For heavier nuclei the diffraction dissociation is larger as a result of a stronger nuclear shadowing.

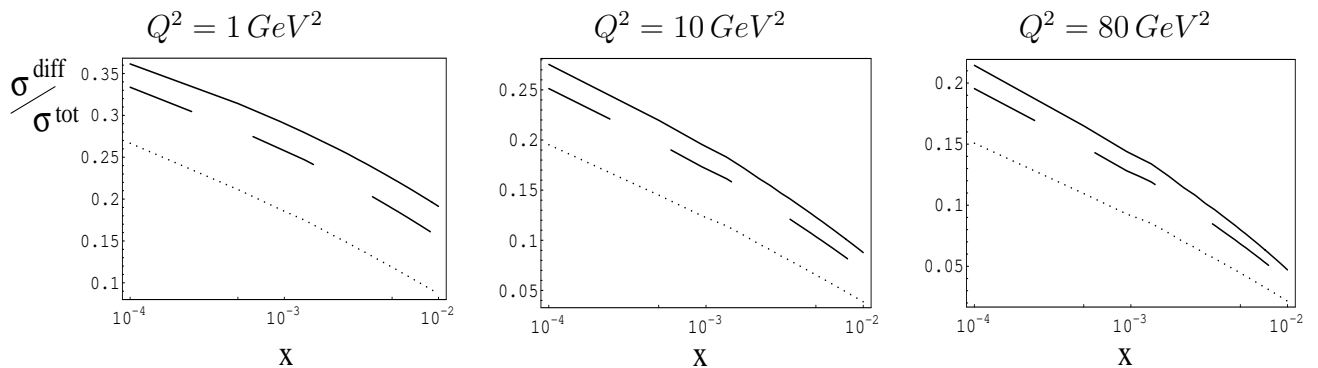


Figure 5: The ratio of inclusive diffractive to total inclusive production is plotted versus x . The curves correspond to Au (solid line), Mo (dashed line), and Ne (dotted line) nuclei.

It is worth now to investigate the A -dependence of the ratio which in perturbative QCD is proportional to $A^{1/3}$ (times the ratio for a proton). We assume the ratio $\sigma^{diff}/\sigma^{tot}$ to preserve the power law dependence on A :

$$\sigma^{diff}/\sigma^{tot} \sim A^{n(x)}.$$

It is clear that in deep saturation regime n should vanish leading to the A -independent behavior, namely the ratio tending to half. Fig. 6 displays the function $n(x)$ for all the nuclei in consideration.

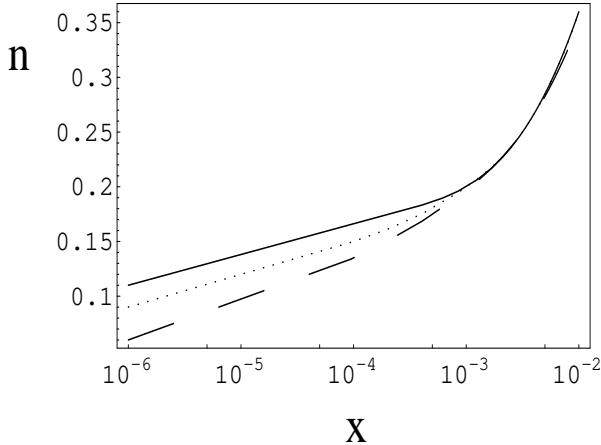


Figure 6: The exponent n is plotted versus x for various values of Q^2 : $Q^2 = 80 \text{ GeV}^2$ (solid line), $Q^2 = 10 \text{ GeV}^2$ (dotted line), and $Q^2 = 1 \text{ GeV}^2$ (dashed line).

It is important to note that the results obtained are in agreement with the results of Ref. [21] where the relevant ratio was considered on a basis of the Glauber-Mueller formula.

6 Theoretical discussion.

One of the most surprising result of our calculations is the geometrical scaling behavior which holds even at sufficiently short distances (large values of photon virtualities Q^2). At short distances the imaginary part of the dipole elastic amplitude has the form

$$N(A; r_\perp, x) \propto r_\perp^2 x G_A(x, \frac{4}{r_\perp^2}) / \pi R_A^2 \approx A^{\frac{1}{3}} r_\perp^2 x G_{proton}(x, \frac{4}{r_\perp^2})$$

The scaling means that this function is a function of only one variable $\tau = r_\perp^2 Q_s^2(A; x)$. Such a nontrivial behavior should certainly result from a kind of conspiracy between three variables r_\perp , x and A . It was shown in Ref. [22] that such a conspiracy occurs between r_\perp and x dependences in a wide range of distances even for large virtualities $Q^2 \approx 4/r_\perp^2 > Q_s^2(A; x)$:

$$Q_s^2 \leq Q^2 \leq Q_s^4/\Lambda^2 \quad (6.20)$$

However, for the geometrical scaling to hold in the case of nuclear targets, an additional condition on the value of the saturation scale is required. Namely, $Q_s^2(A; x) \gg \Lambda^2 A^{\frac{1}{3}}$ in order to justify

the conspiracy between A and the rest of the variables. As was shown in Ref.[23], in the region of low x and large photon virtualities the dipole amplitude looks as follows

$$N(A; \xi = \ln(1/(r_\perp^2 \Lambda^2)), y - y_0 = \ln(x_0/x)) \approx e^{2\sqrt{\tilde{\alpha}_S \xi (y-y_0)} + \xi_A - \xi}, \quad (6.21)$$

where $\xi_A = \frac{1}{3} \ln A$.

The saturation scale can be found from the condition $N = \text{Const}(A, r_\perp, x)$, which leads to the equation for the saturation scale $\xi_s = \ln(Q_s^2/\Lambda^2)$

$$4 \tilde{\alpha}_S \xi_{sat} (y - y_0) = (\xi_{sat} - \xi_A)^2. \quad (6.22)$$

As a result, $\xi_{sat}(y = y_0) = \xi_A$ and $\xi_{sat} = 4 \tilde{\alpha}_S (y - y_0) + 2 \xi_A$ for $\xi_{sat} \gg \xi_A$. Let us expand Eq. (6.21) in the vicinity $Q^2 \approx Q_s^2$ by introducing $\xi = \Delta\xi + \xi_{sat}$ with $\Delta\xi = \ln(Q^2/Q_s^2)$. Considering $\Delta\xi \ll \xi_{sat}$ we get

$$2\sqrt{\tilde{\alpha}_S \xi (y - y_0)} + \xi_A - \xi = -\frac{1}{2} \Delta\xi + \Delta\xi \left(\frac{\xi_A}{\xi_{sat}} \right) + O\left(\left(\frac{\Delta\xi}{\xi_{sat}} \right)^2 \right). \quad (6.23)$$

Therefore, for the scaling behavior to hold we need to assume that

$$\Delta\xi \ll \xi_{sat} \text{ and } \xi_A \ll \xi_{sat}.$$

The first inequality leads to $Q^2 < Q_s^4/\Lambda^2$ while the second one gives $Q_s^2 > \Lambda^2 A^{\frac{1}{3}}$.

In the particular model considered above and at low x , the A dependence of the saturation scale squared is $Q_s^2 \propto A^{\frac{2}{3}}$. For this dependence the second condition just means that x is supposed to be sufficiently small. Our numerical solution, however, shows rather different dependence ($Q_s^2 \propto A^{\frac{1}{3}}$) and the requirement $Q_s^2 > \Lambda^2 A^{\frac{1}{3}}$ has numerical justification only. We would like to recall that the above model is correct at very large photon virtualities only. A natural question arises how to extend this model to smaller virtualities in the range defined by Eq. (6.20). We will discuss this issue below.

The above discussed simple model allowed us to illustrate that the theoretical expectations for the A -dependence of the saturation scale are quite different from the numerical calculations. A possible reason for such different A -dependence is in the fact that $x = 10^{-2} - 10^{-5}$ are not small enough to apply this model. For rather low energies the saturation scale obtained from Eq. (6.22) is proportional to $A^{\frac{1}{3}}$ in agreement with the numerical calculations. In fact, we are still far away from the low x region where the collective effects related to saturation are strong. This can be seen from the ratio $\sigma^{diff}/\sigma^{tot}$ which is not close to the saturation limit $\frac{1}{2}$ and even exhibits some A dependence.

Now, let us try to analyze the diffraction dissociation in DIS using the same approach as in the discussed model. We consider so large initial virtualities that we can restrict ourselves to solution of the linear DGLAP evolution equation. The diagram that contributes to high mass diffraction is shown in Fig. (7). It is well known (see Ref.[24] for example) that this diagram can be written in the form

$$N^D(y - y_0 = \ln M^2, \xi) = \int d\xi' N(y - y_0, \xi - \xi') N^2(y_0, \xi') \quad (6.24)$$

with $N(y - y_0, \xi - \xi')$ given for $\xi - \xi' \gg \xi_{sat}$ by

$$N(y - y_0, \xi - \xi') = \int \frac{df}{2\pi i} e^{\frac{\tilde{\alpha}_S}{f} + (f-1)(\xi - \xi')} \propto e^{2\sqrt{\tilde{\alpha}_S(y-y_0)(\xi - \xi')} - \xi + \xi'} \quad (6.25)$$

and notations shown in Fig. (7). It can be seen that (6.24) is a solution to Eq.(1.5) provided the non-linear terms are neglected in this equation. Moreover, Eq. (6.24) satisfies the correct initial conditions. The non-linear corrections are neglected since we wish to estimate the saturation scale which corresponds to rather small N^D (in semiclassical approach, for example, $N^D \propto \alpha_S$). It is important to emphasize that all A dependence in Eq. (6.24) comes from the initial conditions.

Assuming that the value of x_0 is so small that $N(y_0, \xi')$ is saturated at the saturation scale $\xi' = \xi_{sat}(y_0)$. In this case, the typical value of ξ' in the integrand of Eq. (6.24) is $\xi' = \xi_{sat}(y_0)$. Indeed, for $\xi' < \xi_{sat}(y_0)$ $N(y_0, \xi') \approx \text{const}(y_0, \xi')$ and the main contribution to the integral comes from the upper limit of the integration $\xi' = \xi_{sat}(y_0)$. In the region $\xi' > \xi_{sat}(y_0)$ the integrand falls down as a function of ξ' . As a result, the diffractive amplitude N^D is approximately equal

$$N^D(y - y_0 = \ln M^2, \xi) = N(y - y_0, \xi - \xi_{sat}(y_0)) N^2(y_0, \xi_{sat}) . \quad (6.26)$$

Since $N(y_0, \xi_{sat}) = \text{Const}(y_0)$ we have

$$N^D(y - y_0 = \ln M^2, \xi) \propto e^{2\sqrt{\tilde{\alpha}_S(y-y_0)(\xi - \xi_{sat}(y_0))} - \xi + \xi_{sat}(y_0)} . \quad (6.27)$$

Eq. (6.27) leads to the saturation scale given by the equation

$$4\tilde{\alpha}_S(y - y_0) = \xi_{sat}^D(y) - \xi_{sat}(y_0) . \quad (6.28)$$

Recall that $\xi_{sat}(y_0) = 4\tilde{\alpha}_S y_0 + \xi_A$ ($\xi_{sat}(y_0) \approx \xi_A$) and finally we obtain from Eq. (6.28) that

$$\xi_{sat}^D(y) = 4\tilde{\alpha}_S y + \xi_A . \quad (6.29)$$

It can be seen that this simple approach reproduces our numerical result that the saturation scale for the diffractive production in DIS has the very same x dependence as the saturation scale for the total DIS cross section.

Within the approximations made, $\xi_{sat}^D(y)$ does not depend on y_0 (x_0) in accordance with the numerical calculations. However, we would like to emphasize that the energy dependence for the saturation scale which we obtain from the simple theoretical estimates turns out to be quite different from the numerical results.

At first sight, the A -dependence of the saturation scale in diffractive production appears to be quite different compared to the total cross section. Technically the difference arises from the extra ξ' integration in Eq. (6.24) in comparison with Eq. (6.21). Keeping this in mind we are going

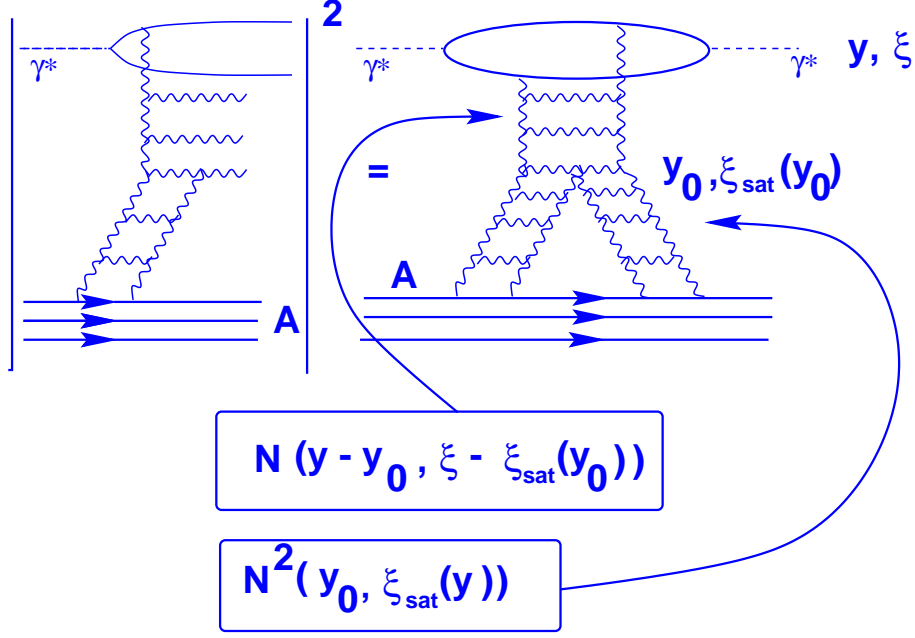


Figure 7: The diffractive production of large mass (M) ($y - y_0 = \ln M^2$) in DIS.

to reconsider saturation in total cross section. To this goal, we can rewrite the dipole amplitude N as an integral over the intermediate virtuality ξ' . As follows from general properties of the DGLAP equation it always can be done.

Fig. (8) displays the picture in which the initial condition for the DGLAP linear evolution is fixed by the McLerran-Venugopalan model (see Ref.[1]). In other words, it is assumed that due to strong gluonic fields in nuclear target at sufficiently low energies (y' in Fig. (8)), a saturation at $Q_s^2(A, y') \gg \Lambda^2$ is reached. In this case the integral over ξ' converges at $\xi' = \xi_{sat}(y')$ and the the dipole amplitude N looks as follows

$$N(A; \xi = \ln(1/(r_\perp^2 \Lambda^2)), y - y' = \ln(x'/x)) \approx e^{2\sqrt{\tilde{\alpha}_S(\xi - \xi_{sat}(y')(y - y') + \xi_{sat}(y') - \xi}}. \quad (6.30)$$

Since for the initial condition for the saturation scale is of the order of $\xi_{sat}(y') \approx \xi_A$, the following expression for the saturation scale is obtained:

$$\xi_{sat}(y) = 4\tilde{\alpha}_S(y - y') + \xi_{sat}(y') = 4\tilde{\alpha}_S(y - y') + \xi_A. \quad (6.31)$$

The saturation scale defined in (6.31) is proportional to $A^{\frac{1}{3}}$ in contrast to (6.22). A natural question arises: what is wrong with the first approach? Eq. (6.21) satisfies all correct initial conditions at short distances. In the integration over ξ' this contribution comes from the upper limit of the integration $\xi' \approx \xi_{sat}$. The the integral over ξ' in the saturation region looks as follows:

$$\int^{\xi_{sat}} d\xi' e^{\xi'} \rightarrow e^{\xi_{sat}}$$

For $\xi' > \xi_{sat}$ the integral is $\int_{\xi_{sat}} d\xi' e^{-\xi'}$. This simple form of the integral is valid in the region $Q^2 > Q_s^4/\Lambda^2$. Of course, this is a small contribution but the estimates in the beginning of this section show that even such a small contribution at sufficiently short distances defined by Eq. (6.22) could reach so large values that we have a dense system of partons.

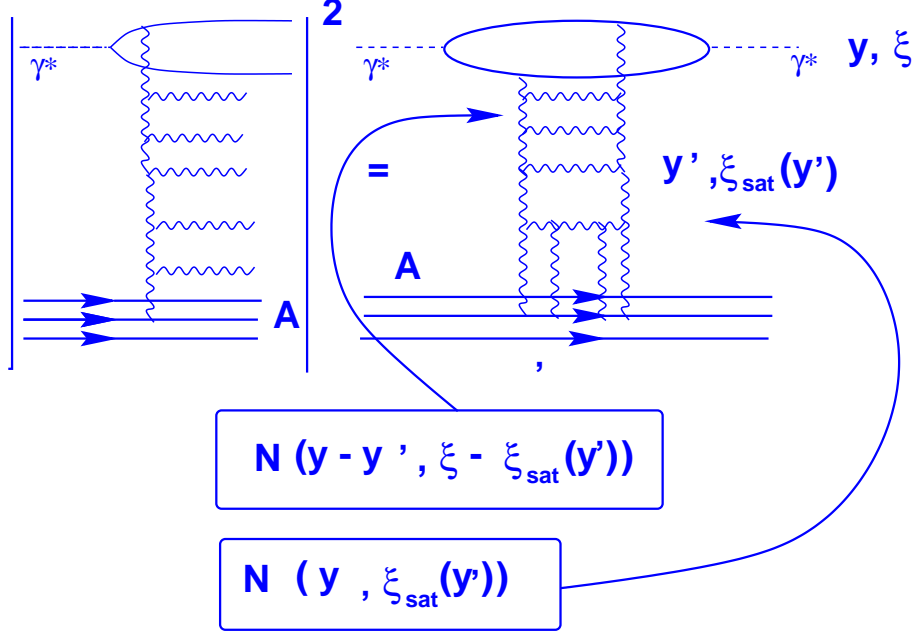


Figure 8: The total cross section for DIS with McLerran-Venugopalan model initial condition.

Actually, Eq. (6.21) is

$$N(A; \xi = \ln(1/(r_\perp^2 \Lambda^2)), y - y_0 = \ln(x_0/x)) = r_\perp^2 A xG(x, \frac{4}{r_\perp^2})/\pi R_A^2 \quad (6.32)$$

in usual notations with xG in double log approximation of pQCD. Eq. (6.32) is correct at least for very short distances.

Eq. (6.30) in the same notations looks differently

$$N(A; \xi = \ln(1/(r_\perp^2 \Lambda^2)), y - y_0 = \ln(x_0/x)) = r_\perp^2 A xG(x, \frac{4}{r_\perp^2 Q_s^2(A; y')})/\pi R_A^2. \quad (6.33)$$

As we have discussed (see Ref. [22] for more details) the geometrical scaling behavior of Eq. (6.33) is preserved till $r_\perp^2 \approx 4\Lambda^2/(A^{\frac{1}{3}} Q_N^4(y'))$. For shorter distances we expect that a new mechanism related to increase of the parton densities inside a nucleon will take over. In this case, the regime discussed in the beginning of this section will be faced with Eq. (6.32) being correct.

To evaluate a typical scale of distances involved we recall that, perhaps, the first RHIC data shows that $Q_s^2(\text{Gold}, x = 10^{-2}) \approx 2 \text{ GeV}^2$ [25]. Therefore, the new regime with $Q_s^2 \propto A^{\frac{2}{3}}$ is expected to start at $r_\perp^2 < 0.01 \text{ GeV}^{-2} = 4 \cdot 10^{-4} \text{ fm}^2$. As can be seen in Fig. (1) the diffraction amplitude is far away from the saturation region at so short distances and at $x = 10^{-2} - 10^{-6}$.

7 Conclusions

The non-linear evolution equation (1.5) is solved numerically for six real nuclear targets Ne_{20} , Ca_{40} , Zn_{70} , Mo_{100} , Nd_{150} , and Au_{197} . The solutions obtained display the very same pattern as in the case of proton target [16]. These solutions are used to study the A -dependence of single diffractive dissociation.

The saturation scale $Q_{s,A}^D$ is estimated. The fit to the parameterization $Q_s^D(A, x, x_0) \sim A^p x^{-\lambda}$ reveals powers p and λ . The results on λ coincide with the corresponding power obtained for the proton case [16] while the A -dependence is the same as found for the saturation scale $Q_{s,A}$ - saturation scale obtained in total production [12]. The function $Q_{s,A}^D$ is found to be almost independent on x_0 .

The geometrical scaling with respect to x is well established for all nuclei considered. The scaling holds within a few percent accuracy and in the whole kinematic region investigated. As a consequence, inclusive diffractive production off nuclei is predicted to possess the scaling both with respect to x and A . Like for the proton target the scaling phenomena with respect to x_0 set in at $x \ll x_0$ but is violated at $x \sim x_0$.

As we have discussed in the previous section we can explain theoretically the A and x_0 dependence of the calculated saturation scale but the x dependence is too smooth in comparison with theoretical estimates.

The ratio of $\sigma^{diff}/\sigma^{tot}$ was examined on a basis of the solutions obtained. At $x \simeq 10^{-4}$ a significant shadowing is expected of order 25% and it is larger for heavy nuclei.

The fact that this ratio turns out to be very close to the estimates based on the Glauber-Mueller formula [21], shows that we can use the latter as a simple approach for the first evaluation of the possible collective effects in the saturation region of high parton density QCD.

Acknowledgements: The authors wish to thank the DESY and Hamburg University Theory Groups for their hospitality and creative atmosphere during several stages of this work. Our special thanks go to Asher Gotsman, Uri Maor and Eran Naftali for very stimulating discussion on the subject of this paper.

Part of this work done by M.L. was performed in the Technion. M.L. is very grateful to Physics Department of the Technion and especially to the members of the High Energy Group for warmth and creative atmosphere.

This research was supported in part by the BSF grant # 9800276, by the GIF grant # I-620-22.14/1999 and by Israeli Science Foundation, founded by the Israeli Academy of Science and Humanities.

References

- [1] L. V. Gribov, E. M. Levin, and M. G. Ryskin, *Nucl. Phys. B* **188** (1981) 555, *Phys. Rep.* **100** (1983) 1; A. H. Mueller and J. Qiu, *Nucl. Phys. B* **268** (1986) 427; L. McLerran and

- R. Venugopalan, *Phys. Rev. D* **49** (1994) 2233, 3352; **D 50** (1994) 2225, **D 53** (1996) 458, **D 59** (1999) 094002; E. Levin and M.G. Ryskin, *Phys. Rep.* **189** (1990) 267; J. C. Collins and J. Kwiecinski, *Nucl. Phys. B* **335** (1990) 89; J. Bartels, J. Blumlein, and G. Shuler, *Z. Phys. C* **50** (1991) 91; E. Laenen and E. Levin, *Ann. Rev. Nucl. Part. Sci.* **44** (1994) 199 and references therein; Yu. Kovchegov, *Phys. Rev. D* **54** (1996) 5463, **D 55** (1997) 5445, **D 61** (2000) 074018; A. L. Ayala, M. B. Gay Ducati, and E. M. Levin, *Nucl. Phys. B* **493** (1997) 305, **B 510** (1998) 355 A. H. Mueller, *Nucl. Phys. B* **572** (2000) 227, **B 558** (1999) 285; J. Jalilian-Marian, A. Kovner, L. McLerran, and H. Weigert, *Phys. Rev. D* **55** (1997) 5414; J. Jalilian-Marian, A. Kovner, and H. Weigert, *Phys. Rev. D* **59** (1999) 014015; J. Jalilian-Marian, A. Kovner, A. Leonidov, and H. Weigert, *Phys. Rev. D* **59** (1999) 034007, Erratum-ibid. *Phys. Rev. D* **59** (1999) 099903; A. Kovner, J. Guilherme Milhano, and H. Weigert, *Phys. Rev. D* **62** (2000) 114005; H. Weigert, *Nucl. Phys. A* **703** (2002) 823.
- [2] Yu. Kovchegov, *Phys. Rev. D* **61** (2000) 074018; E. Levin and K. Tuchin, *Nucl. Phys. B* **573** (2000) 833; **A 691** (2001) 779; E. Ferreira, E. Iancu, K. Itakura and L. McLerran, hep-ph/0206241, *Nucl. Phys. A* **703** (2002) 489; E. Iancu, A. Leonidov and L. McLerran, *Nucl. Phys. A* **692** (2001) 583, *Phys. Lett. B* **510** (2001) 133.
- [3] Yu. Kovchegov and L. McLerran, *Phys. Rev. D* **60**, 054025 (1999).
- [4] V.A. Abramovski, V.N. Gribov and O.V. Kancheli, *Sov. J. Nucl. Phys.* **18** (1974) 308; J. Bartels and M.G. Ryskin, *Z. Phys. C* **76** (1997) 241, hep-ph/9612226 and references therein.
- [5] A. H. Mueller, *Nucl. Phys. B* **415** (1994) 373.
- [6] A. H. Mueller, *Nucl. Phys. B* **335** (1990) 115.
- [7] N. N. Nikolaev and B. G. Zakharov, *Z. Phys. C* **49** (1991) 607; E. M. Levin, A. D. Martin, M. G. Ryskin, and T. Teubner, *Z. Phys. C* **74** (1997) 671.
- [8] Ia. Balitsky, *Nucl. Phys. B* **463** (1996) 99.
- [9] Yu. Kovchegov, *Phys. Rev. D* **60** (2000) 034008.
- [10] M. Braun, *Eur. Phys. J. C* **16** (2000) 337; N. Armesto and M. Braun, *Eur. Phys. J. C* **20** (2001) 517; K. Golec-Biernat, L. Motyka, and A. M. Stasto. *Phys. Rev. D* **65** (2002) 074037.
- [11] M. Lublinsky, E. Gotsman, E. Levin, and U. Maor, *Nucl. Phys. A* **696** (2001) 851.
- [12] E. Levin and M. Lublinsky, *Nucl. Phys. A* **696** (2001) 833.
- [13] Yu. Kovchegov and E. Levin, *Nucl. Phys. B* **577** (2000) 221.
- [14] A. Kovner and U. A. Wiedemann *Phys. Rev. D* **64** (2001) 114002.
- [15] ZEUS Collaboration, J. Breitweg et al., *Eur. Phys. J. C* **6** (1999) 43; H1 Collaboration, C. Adloff et al., *Z. Phys. C* **76** (1997) 613.

- [16] E. Levin and M. Lublinsky, *Europ. Phys. J. C* **22** (2002) 647.
- [17] E. Levin and M. Lublinsky, *Phys. Lett. B* **521** (2001) 233.
- [18] C. W. De Jagier, H. De. Vries, and C. De Vries, *Atomic Data and Nuclear Data Tables* **Vol. 14** No 5, 6 (1974) 479.
- [19] K. Golec-Biernat, J. Kwiecinski, and A. M. Stasto, *Phys. Rev. Lett.* **86** (2001) 596.
- [20] M. Lublinsky, *Europ. Phys. J. C* **21** (2001) 513.
- [21] E. Gotsman, E. Levin, M. Lublinsky, U. Maor, and K. Tuchin, *Nucl. Phys. A* **697** (2002) 521; *Phys. Lett. B* **492** (2000) 47.
- [22] E. Iancu, K. Itakura and L. McLerran, [hep-ph/0203137](#).
- [23] E. Levin and K. Tuchin, *Nucl. Phys. A* **693** (2001) 787
- [24] E. Levin and M. Wusthoff, *Phys. Rev. D* **50** (1994) 4306 and references therein.
- [25] D. Kharzeev and M. Nardi, *Phys. Lett. B* **507** (2001) 121; D. Kharzeev and E. Levin, *Phys. Lett. B* **523** (2001) 79; D. Kharzeev, E. Levin and M. Nardi, [hep-ph/0111315](#).